iScience

CellPress
OPEN ACCESS

Article

Highly solar reflectance and infrared transparent porous coating for non-contact heat dissipations

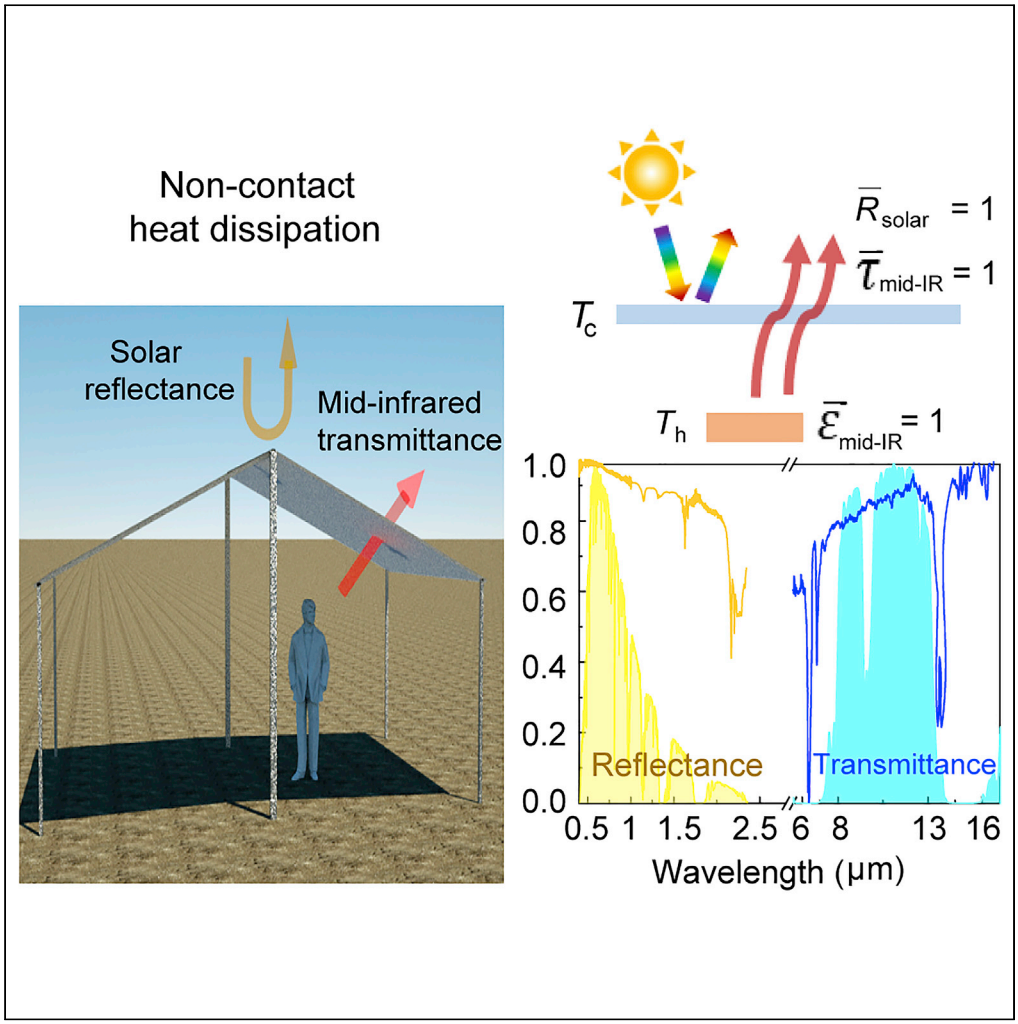

Meijie Chen, Dan Pang, Hongjie Yan

chenmeijie@csu.edu.cn (M.C.)
s-rfy@csu.edu.cn (H.Y.)

Highlights

Infrared transparent coating was used for non-contact heat dissipations

High solar reflectance $\overline{R}_{solar}$ and IR-transmittance $\overline{\tau}_{LWIR}$ can be 0.96 and 0.88

IR transparent coating obtained a 4°C lower heater temperature than normal coating

Chen et al., iScience 25, 104726
August 19, 2022
https://doi.org/10.1016/j.isci.2022.104726

iScience

CellPress
OPEN ACCESS

Article

Highly solar reflectance and infrared transparent porous coating for non-contact heat dissipations

Meijie Chen,[1,2,*] Dan Pang,[1] and Hongjie Yan[1,*]

SUMMARY

Passive daytime radiative cooling (PDRC) can dissipate heat to outer space with high solar reflectance ($\overline{R}_{solar}$) and thermal emittance ($\overline{\varepsilon}_{LWIR}$) in the atmospheric transmission window. However, for the non-contact heat dissipation, besides the high $\overline{R}_{solar}$, a high infrared transmittance ($\overline{\tau}_{LWIR}$) is needed to directly emit thermal radiation through the IR-transparent coating to outer space. In this work, An IR-transparent porous PE (P-PE) coating with $\overline{R}_{solar}$= 0.96 and $\overline{\tau}_{LWIR}$= 0.88 was prepared for non-contact heat dissipations. Under the direct sunlight of 860 W m^{-2}, the IR-transparent coating obtained a 4°C lower heater temperature than the normal PDRC coating under the same condition. In addition, the spectral reflectance of the P-PE coating after immersing in air or water changed little, which showed excellent durability for long-term outdoor applications. These results indicate the P-PE coating can be a potential IR-transparent coating for non-contact heat dissipations under direct sunlight.

INTRODUCTION

Passive daytime radiative cooling (PDRC) as an innovative alternative cooling technology achieves a cool surface by emitting thermal radiation to outer space and avoiding solar heating without energy input. It can effectively reduce energy consumption through refrigeration (Liu et al., 2021; Mahian et al., 2021; Chen et al., 2020, Chen et al., 2021a, 2022) and mitigate the urban heat island effect and pollution (Yang and Zhang, 2020; Mandal et al., 2020; Zhao et al., 2019; Zhong et al., 2021; Raman et al., 2014; Liu et al., 2019). A normal PDRC coating can achieve a sub-ambient temperature by modifying its surface to have a high solar reflectance ($\overline{R}_{solar}$) in the wavelength of 0.3–2.5 μm to minimize solar heat gain under direct sunlight (Kou et al., 2017; Zhu et al., 2013; Xiang et al., 2021) and high emittance ($\overline{\varepsilon}_{LWIR}$) in the long-wavelength infrared (LWIR) atmospheric transmission window (Li et al., 2020a; Chen et al., 2021a) to directly radiates excess heat to outer space at a temperature of ~3 K (Leroy et al., 2019; Mandal et al., 2018; Zhang et al., 2021a; Zhang et al., 2022).

Remarkable progress has been made recently to achieve PDRC by the normal PDRC coatings (Zhao et al., 2022; Cheng et al., 2021; Weng et al., 2021; Zhang et al., 2020; Wang et al., 2021). The spectrum manipulations for normal PDRC coatings were realized by various structures (Zhai et al., 2017; Chen et al., 2016; Yu et al., 2020; Fuqiang, 2020). Normal PDRC coatings can efficiently cool the object in direct contact (Zhou et al., 2019; Huang and Ruan, 2017; Atiganyanun et al., 2018; Li et al., 2020b), while in non-contact heat dissipations, the encapsulated air with a low thermal conductivity between coatings and objects would weaken the cooling performance. Therefore, a scalable and inexpensive IR-transparent ($\overline{\tau}_{LWIR}$) coating is needed to transfer the infrared thermal radiation through the IR coating and atmospheric window to outer space, which is suitable for non-contact heat dissipations have been proposed (Kim and Lenert, 2018; Tian et al., 2021).

Polyethylene (PE) is semi-transparent in the mid-infrared owing to the low absorption by the polyethylene backbone (Leroy et al., 2022), and once made into a mesoporous structure where the mismatch in refractive indices between air and PE amplifies light scattering achieves high $\overline{R}_{solar}$ (Chen et al., 2021a; Cao et al., 2022). The unusual combination of high $\overline{R}_{solar}$ and $\overline{\tau}_{LWIR}$ of porous PE (P-PE) are promising for non-contact heat dissipations (Cai et al., 2018; Hsu et al., 2016). However, there remains a challenge to the IR-transparent coating because $\overline{\tau}_{LWIR}$ increases with decreasing the thickness while solar heating increases owing to the low solar reflectance at small thicknesses. Micrometer-sized pores of polyethylene aerogel (PEA) which is a high-porosity material made of polyethylene can cause strong light scattering in the solar

[1]School of Energy Science and Engineering, Central South University, Changsha 410083, China

[2]Lead contact

*Correspondence: chenmeijie@csu.edu.cn (M.C.), s-rfy@csu.edu.cn (H.Y.)

https://doi.org/10.1016/j.isci.2022.104726

spectrum leading to a high $\overline{R}_{solar}$. However, the PEA is usually millimeter thick resulting in an IR-transparent of less than 80% (A. Leroy et al., 2019). How to balance $\overline{R}_{solar}$ and $\overline{\tau}_{LWIR}$ and make sure the mechanical and stability performance of the P-PE coating at a small thickness by mixing the high-density polyethylene (HDPE) and ultra-high molecular weight PE (UHMWPE) is still a challenge for non-contact heat dissipation applications.

In this work, we firstly theoretically demonstrated the advantages of non-contact heat dissipations by IR-transparent coating and fabricated P-PE coatings by utilizing the thermally induced phase separation method. After process parameters optimization, the P-PE coating demonstrates simultaneously high solar reflectance (0.96) and infrared transmittance (0.88) at a thin thickness of 100 μm. After being exposed to the air and immersed in water, $\overline{R}_{solar}$ of P-PE coating still can reach more than 0.95. The thermal measurement under an averaged solar intensity (I_{solar}) of 860 W m^{-2} shows that the rubber temperature drops nearly 15°C with P-PE coating and the cooling performance of P-PE coating is better than that of normal PDRC coating which only achieves a temperature of 11°C below the rubber, indicating that IR-transparent coatings have a better heat dissipation performance. In addition, the perfect waterproof and mechanical properties of P-PE coating would help the coating for long-term outdoor applications.

RESULTS

Principle of non-contact heat dissipations

PDRC shows great interest in outdoor cooling or heat dissipation. Normal PDRC with high $\overline{R}_{solar}$ and $\overline{\varepsilon}_{LWIR}$ can efficiently cool the object in direct contact (Zhao et al., 2022) While in non-direct contact (such as sun-shade), the air between the coating and object would block the heat dissipation owing to the low thermal conductivity of air (0.023 W m^{-1} K^{-1}).

To enhance the non-contact heat dissipation performance, an IR transparent coating is needed with the high $\overline{R}_{solar}$ and $\overline{\tau}_{LWIR}$ (Figure 1A) as lots of objects (such as oxides, minerals, glasses, water, skin, and so on) have a high thermal emittance >0.4 except for some polished metals with a small emittance <0.4 (Incropera and Dewitt, 2002). Compared with the normal PDRC, the object under the IR transparent coating can emit radiative power through the IR transparent coating to the outer space directly for heat dissipation (Figure 1B), the ideal spectrum for the IR transparent coating achieves $\overline{R}_{solar}$= 1 and $\overline{\tau}_{LWIR}$ = 1. Although in the normal PDRC (ideal $\overline{R}_{solar}$= 1 and $\overline{\varepsilon}_{LWIR}$ = 1), it only emits radiative power to the coating and then transfers to the outer space, which greatly increases thermal resistance (Figures 1D and 1E). Detailed calculation about the $\overline{R}_{solar}$, $\overline{\varepsilon}_{LWIR}$, and $\overline{\tau}_{LWIR}$ can be found in method details.

Simulation of heat dissipation performance

Firstly, the heat dissipation performance based on the IR transparent and normal PDRC coatings is simulated based on the model in Figure 2A. The air is filled between the PDRC coating and the heater for non-contact heat dissipation. Ideal spectra in Figures 1C and 1E are used for this simulation without special marks, i.e., ideal normal PDRC: R = 1 for λ = 0.3–2.5 μm and ε = 1 for λ > 8 μm; IR-transparent coating: R = 1 for λ = 0.3–2.5 μm and τ= 1 for λ > 8 μm. Detailed simulation can be found in method details.

Thermal emittance of the heater in the confined space has a great effect on the heat dissipation performance. Increasing the heater emittance would greatly decrease the heater temperature T_h (Figure 2B). And the IR transparent coating achieves a lower heater temperature than the normal PDRC coating as the heating power can be dissipated to outer space directly through the IR transparent coating. For example, at a heating power of 200 W m^{-2}, the heater temperature based on the IR transparent coating can be 15 and 22°C lower than the normal coating at the heater emittance 0.4 and 0.9, respectively. And the common objects (such as oxides, minerals, glasses, water, skin, and so on) have a high thermal emittance >0.4 (Incropera and Dewitt, 2002).

When the heat power increases from 100 W m^{-2} to 1000 W m^{-2}, the heater temperature under the normal coating increases from 41°C to 164°C, while the heater temperature based on the IR transparent coating increases from 23°C to 116°C (Figure 2C). The temperature of the normal coating increases rapidly from 23°C to 86°C while the IR transparent coating maintains at ~ 26°C owing to the thermal insulation of the air layer and the IR transparent (Figure 2D). The simulation results show the IR transparent coating has a better cooling performance than the normal PDRC coating in the non-contact heat dissipation.

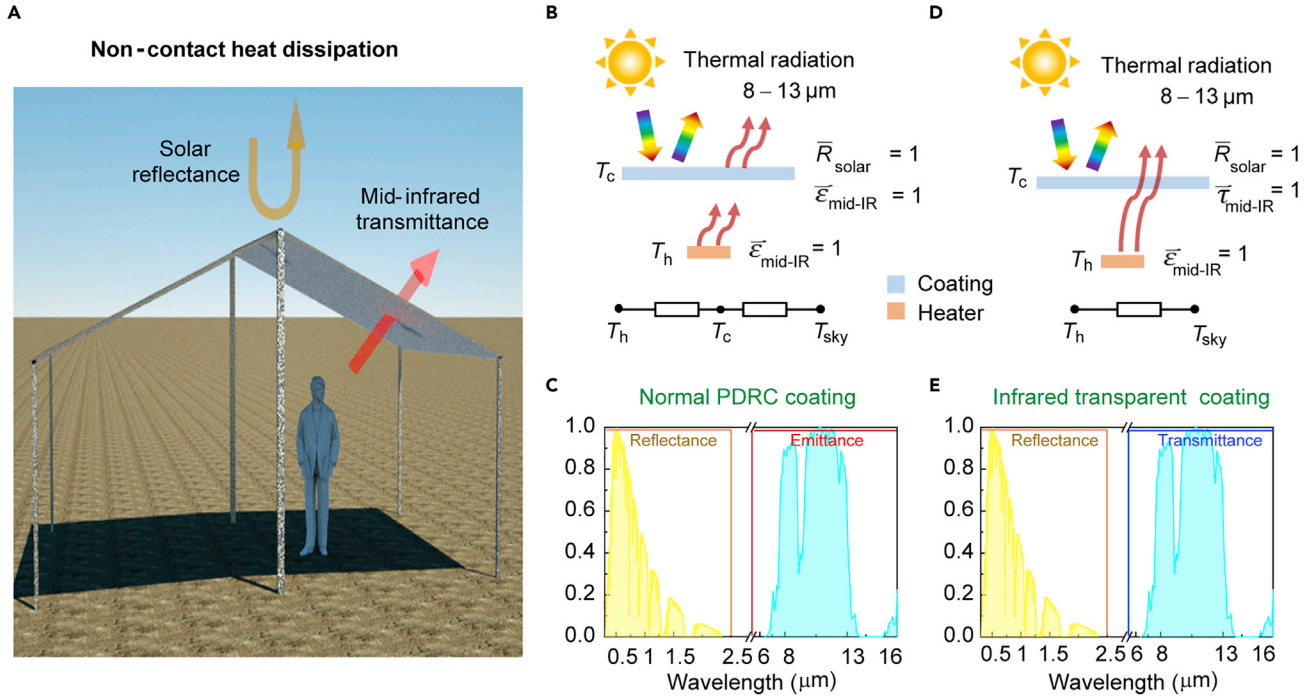

Figure 1. Principle of the IR transparent coating for non-contact heat dissipations

(A) Schematic diagram of non-contact heat dissipation, such as sunshade.

(B) Heat transfer processes in the ideal normal PDRC with (C) the high $\overline{R}_{solar}$ and $\overline{\varepsilon}_{LWIR}$ to minimize solar heating and emit radiative power to outer space, and the inner heater emits radiative power to the PDRC coating.

(D) Heat transfer processes in the ideal IR-transparent coating with (E) the high $\overline{R}_{solar}$ and $\overline{\tau}_{LWIR}$ can depress simultaneously heat gain from solar and the heater can emit radiative power to outer space through the IR transparent coating directly.

Design of infrared-transparent coatings

PE is a potential material used in the IR-transparent coating owing to its low imaginary part $k \sim 0$ of the complex refractive index (Smith and Loewenstein, 1975). Inserting nano-sized scatters into PE can efficiently reflect solar radiation while maintaining a high IR transmittance owing to the little IR scattering ability of nano-sized scatters and the little IR absorptance of PE. However, a thickness of 300–500 μm is usually needed to achieve a high solar reflectance (Li et al., 2020b; Mandal et al., 2018; Ma et al., 2021; Zhang et al., 2021b), which is too large for the IR-transparent coating and would weaken the IR transmittance. The key issue for IR-transparent coatings is to achieve high solar reflectance at a small thickness (such as ~ 100 μm). Here the P-PE coating as the IR-transparent coating is prepared using paraffin oil to mix the high-density PE (HDPE) and ultra-high molecular weight PE (UHMWPE) and then the cooled mixture is melt-pressed to form thin films. Finally, the P-PE can be achieved by extracting the paraffin oil with ethanol. Detailed preparation information can be found in method details.

Based on the Mie scattering theory, the nanopore size and density strongly determine the scattering ability or reflectivity of the porous structure in the solar spectrum (Chen et al., 2021b), which can be tuned by changing the mass ratio of HDPE and UHMWPE (m_{HDPE}/m_{UHMWPE}), and the paraffin oil mass concentration (ω_{oil}) (Leroy et al., 2022; Peng et al., 2018). It can be found that the value of m_{HDPE}/m_{UHMWPE} has little effect on the mid-infrared transmittance owing to the small thickness of ~100 μm, and the largest solar reflectance can be achieved at m_{HDPE}/m_{UHMWPE} = 7/3 (Figure 3A). Similarly, the value of ω_{oil} also has little effect on the mid-infrared transmittance at a thickness of 100 μm. A too large or small value of ω_{oil} would weaken the solar reflectance and the largest solar reflectance can be obtained at ω_{oil}= 81% (Figure 3B).

The hot-pressing temperature (T) also can affect thermal-induced phase separation. Increasing T would decrease the mid-infrared transmittance (Figure 3C), which can be chosen as 130°C as a too low

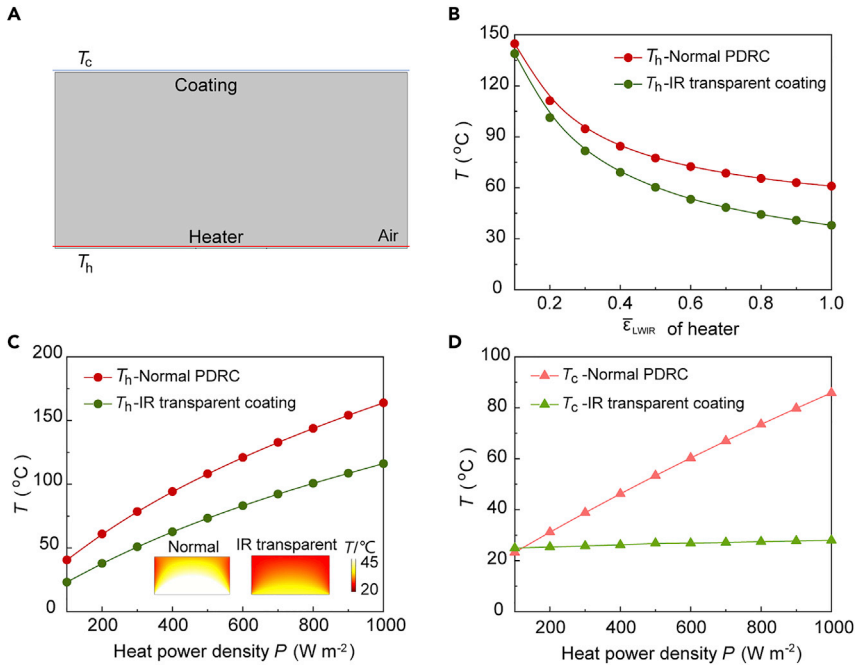

Figure 2. Simulation of heat dissipation performance

(A) Simulation model diagram of heat dissipation.

(B) The heater temperature with different heater emittances under normal (red) and IR-transparent (green) coatings at a heat resource power density (200 W m^{-2}).

(C) Heater temperatures and (D) coating temperature based on normal (red) and IR-transparent (green) coatings at a heat power from 100 W m^{-2} to 1000 W m^{-2}. The insert in (C) shows the temperature distributions under a normal and IR-transparent coating with a heat resource power density (200 W m^{-2}). The heater emittance is one for (C) and (D).

temperature would make it difficult to form the thin film. On the other hand, increasing the thickness would also reduce the mid-infrared transmittance (Figure 3D). To balance the solar reflectance and mid-infrared transmittance, the coating thickness can be determined as 100 μm, and $\overline{R}_{solar}$= 0.96 and $\overline{\tau}_{LWIR}$= 0.88 can be achieved at ω_{oil}= 81% and m_{HDPE}/m_{UHMWPE} = 7/3. Compared with the commercial white PE coating with $\overline{R}_{solar}$= 0.85 and $\overline{\tau}_{LWIR}$= 0.75 at a thickness of 100 μm (Figure S1), the prepared P-PE coating in this work shows great solar reflectance and mid-infrared transmittance, which can be a potential coating for the non-contact heat dissipations.

DISCUSSION

Durability and mechanical properties of infrared-transparent coatings

Owing to the strong scattering ability of pores in the PE coating, it shows opaque at a small thickness of 100 μm (Figure 4A). To further demonstrate the durability of the P-PE coating, the solar spectral reflectance is measured before and after it is exposed in the air for 14 days and immersed in water for 24 h. Results show that there is nearly no decline in $\overline{R}_{solar}$, which still can reach more than 0.95 (Figure 4B), indicating the excellent durability of the P-PE coating for long-term outdoor applications.

As an IR-transparent coating for outdoor heat dissipations, it is also important to avoid water penetration at a such small coating thickness, which can protect objects under the coating from wetting. Water vapor transmission experiments are conducted to characterize the waterproof coatings (Figure 4C). Under the same condition, the water vapor evaporation mass reaches 0.18 and 3.1g after 24 h with the P-PE coating or not, respectively. The water vapor transmission rate (WVTR) of the P-PE coating only reaches 0.0015 g h^{-1}·cm^{-2}. In addition, the P-PE coating can reach up to 485% deformation with great flexibility owing to the high mass ratio of UHMWPE (Figure 4D). These results show that the P-PE coating has great durability and mechanical properties, which can be a potential IR-transparent coating for outdoor applications. Detailed information about these experiments can be found in method details.

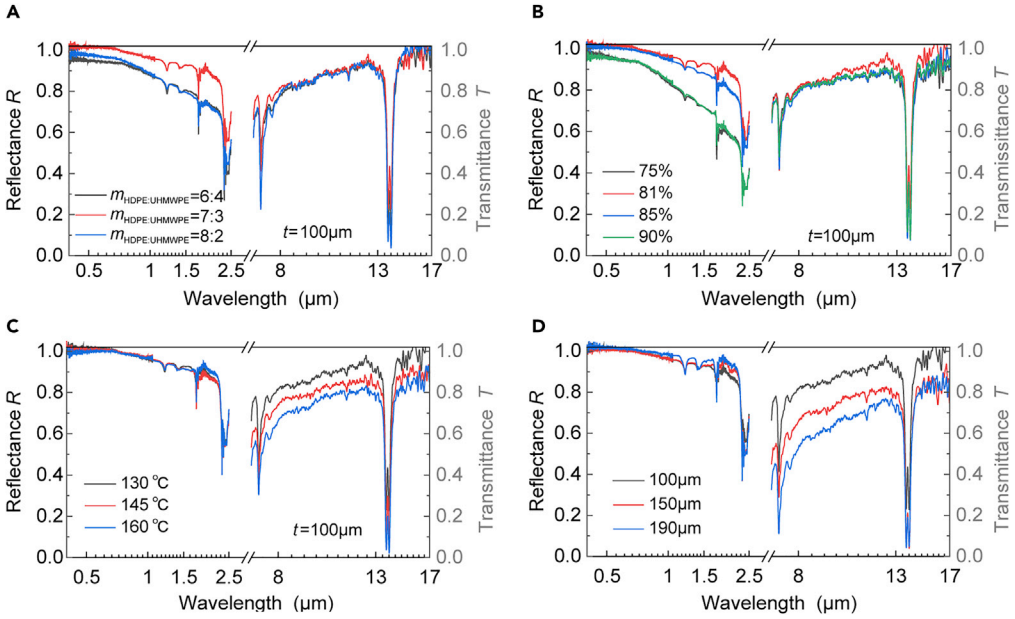

Figure 3. Design of IR-transparent coatings

Spectral reflectance and transmittance of P-PE coatings with different (A) mass ratios of HDPE and UHMWPE (ω_{oil} = 81%, T = 130°C and t = 100 μm), (B) oil content (m_{HDPE}/m_{UHMWPE} = 7/3, T = 130°C and t = 100 μm), (C) hot pressing temperature (m_{HDPE}/m_{UHMWPE} = 7/3, ω_{oil}= 81%, and t = 100 um), and (D) thicknesses (m_{HDPE}/m_{UHMWPE} = 7/3, ω_{oil}= 81%, and T = 130°C).

Outdoor cooling performance

Finally, the outdoor experiments are conducted to investigate the heat dissipation performance of normal PDRC and IR-transparent P-PE coatings (Figure 5A). To achieve the same similar solar reflectance $\overline{R}_{solar}$= 0.96, a Polydimethylsiloxane (PDMS) layer is fixed under the P-PE coating to achieve the normal PDRC coating (Figure 5B). It can be found that the normal PDRC coating achieve $\overline{\varepsilon}_{LWIR}$= 0.85, which is slightly smaller than the common PDMS film owing to the mid-infrared reflectance of the P-PE coating (Figure S2). Silicone rubber is used for the heater that needs heat dissipation, which has $\overline{\varepsilon}_{LWIR}$= 0.94 (Figure 5B). Detailed outdoor experiment information can be found in method details.

Under direct sunlight (~860 W m^{-2} in Figure 5C), the bare silicone rubber without any coatings is ~12°C higher than the air temperature owing to the low $\overline{R}_{solar}$~ 0.22 (Figure 5D). By covering a normal PDRC coating on the silicone rubber, its temperature can drop ~11°C compared with the case without any coating owing to the high $\overline{R}_{solar}$ and $\overline{\varepsilon}_{LWIR}$ of the normal coating. Further, with the IR-transparent P-PE coating as a shield, the silicone rubber temperature drops ~15°C as the high $\overline{\tau}_{LWIR}$ allows the radiative power emits to outer space through the IR-transparent coating. In addition, under an averaged solar intensity of 923 W m^{-2}, when the heat power density increase from 370 W m^{-2} to 655 W m^{-2}, the silicone rubber temperature only increases from 47°C to 62°C, which is similar to the simulation results (Figure 2C) and shows the great heat dissipation performance at different heat powers (Figure S3). Based on the above results, the P-PE coating can be a potential IR-transparent coating for non-contact heat dissipations.

In conclusion, we theoretically and experimentally demonstrated the IR-transparent coating for non-contact heat dissipations. Compared with the normal PDRC coating with the high $\overline{R}_{solar}$ and $\overline{\varepsilon}_{LWIR}$, the IR-transparent coating with the high $\overline{R}_{solar}$ and $\overline{\tau}_{LWIR}$ efficiently cooled the heater by emitting radiative power from the heater to outer space through the IR-transparent coating. To balance the solar reflectance and mid-infrared transmittance, $\overline{R}_{solar}$= 0.96 and $\overline{\tau}_{LWIR}$= 0.88 were achieved for the P-PE coating experimentally at t = 100 μm, ω_{oil}= 81%, and m_{HDPE}/m_{UHMWPE} = 7/3. Under the direct sunlight of 860 W m^{-2}, the IR-transparent coating obtained a 4°C lower heater temperature than the normal PDRC coating under the same condition.

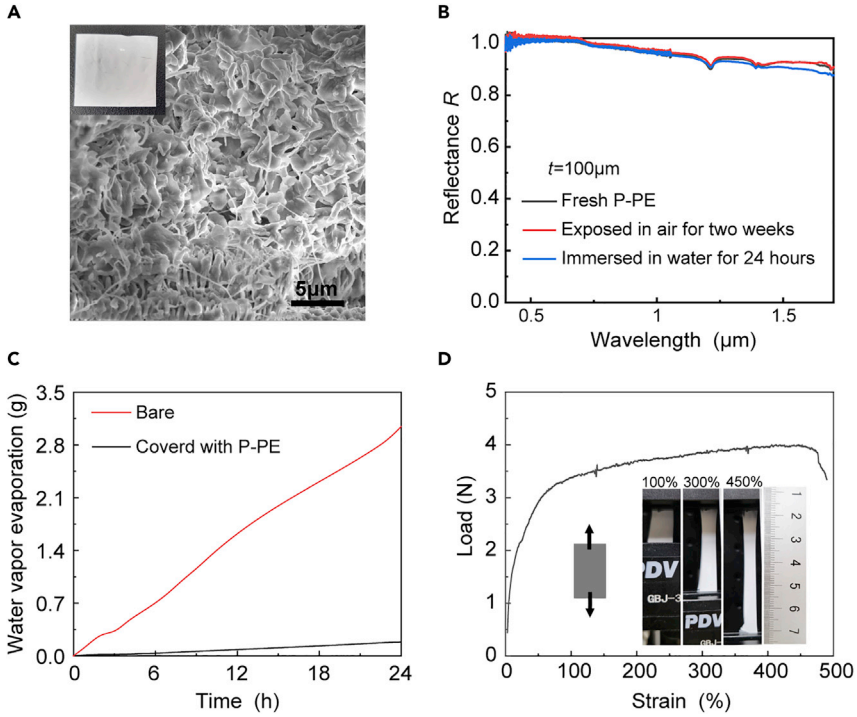

Figure 4. Durability and mechanical properties of IR-transparent coatings

(A) SEM image of the P-PE coating and the inset is an optical image at a thickness of 100 μm.

(B) Reflectance spectra of the P-PE coating exposed in the air (red), immersed in water for 24h (blue), and fresh coating (black).

(C) Water vapor evaporation with the P-PE coating (black) and without coating (red).

(D) A stretching test of the P-PE coating (width: 1cm and thickness: 100 μm).

Limitations of the study

Although the non-contact heat dissipation can be enhanced by the highly solar reflectance and mid-infrared transmittance porous coating under sunlight. The infrared transmittance is still limited to balance the solar reflectance. More efforts based on photonics and materials design are still needed to improve solar reflectance with an ultra-thin coating. In addition, methods such as electrospinning are recommended for large-scale applications in further study.

STAR★METHODS

Detailed methods are provided in the online version of this paper and include the following:

- KEY RESOURCES TABLE
- RESOURCE AVAILABILITY
  - Lead contact
  - Materials availability
  - Data availability
- METHOD DETAILS
  - Preparation of P-PE coatings
  - Sample characterizations
  - Water vapor transmission property tests
  - Field tests
  - Heat dissipation calculation

SUPPLEMENTAL INFORMATION

Supplemental information can be found online at https://doi.org/10.1016/j.isci.2022.104726.

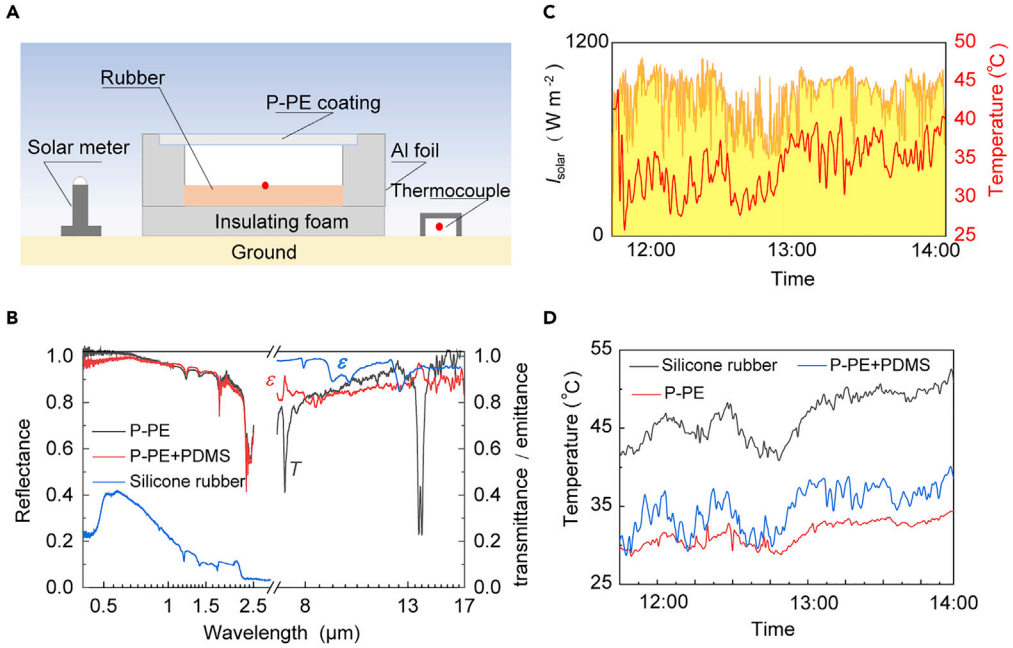

Figure 5. Outdoor cooling performance of P-PE coatings

(A) Schematic of the outdoor cooling performance experiment device.

(B) Spectral of P-PE coating (black: shows the reflectance and transmittance of P-PE coating), P-PE + PDMS coating (red: shows the reflectance and emittance of P-PE + PDMS coating), and silicone rubber (red: shows the reflectance and emittance of silicone rubber).

(C) Real-time I_{solar} and temperature measurements of air.

(D) Real-time temperatures of silicone rubber without any coating (black), with the P-PE coating (red), and P-PE + PDMS coating (blue). Wind velocity: 3.4 m s^{-1}-5.4 m s^{-1}. Location: Changsha, Hunan province, China. Date: 2022-five to two.

ACKNOWLEDGMENTS

This work was financially supported by the National Natural Science Foundation of China (Grant No. 52006246) and the Natural Science Foundation of Hunan Province (Grant No. 2021JJ40732).

AUTHOR CONTRIBUTIONS

M. C. conceived the idea and designed the simulations and experiments, reviewed and revised the article. D. P. carried out various aspects of the simulations and experiments and wrote the article. H. Y. supervised the work.

DECLARATION OF INTERESTS

The authors declare no competing interests.

Received: June 7, 2022
Revised: June 22, 2022
Accepted: June 29, 2022
Published: August 19, 2022

REFERENCES

Atiganyanun, S., Plumley, J.B., Han, S.J., Hsu, K., Cytrynbaum, J., Peng, T.L., Han, S.M., and Han, S.E. (2018). Effective radiative cooling by paint-format microsphere-based photonic random media. ACS Photonics *5*, 1181–1187. https://doi.org/10.1021/acsphotonics.7b01492.

Cai, L., Song, A.Y., Li, W., Hsu, P.C., Lin, D., Catrysse, P.B., Liu, Y., Peng, Y., Chen, J., Wang, H., et al. (2018). Spectrally selective nanocomposite textile for outdoor personal cooling. Adv. Mater. *30*, e1802152. https://doi.org/10.1002/adma.201802152.

Cao, D., Li, X., and Gu, Y. (2022). Highly optically selective polyethylene porous films as versatile optical shields for daytime radiative cooling applications. Sol. Energy Mater. Sol. Cells *240*, 111727. https://doi.org/10.1016/j.solmat.2022.111727.

Chen, M., Pang, D., Chen, X., and Yan, H. (2021a). Investigating the effective radiative cooling performance of random dielectric microsphere coatings. Int. J. Heat Mass Transf. *173*, 121263. https://doi.org/10.1016/j.ijheatmasstransfer.2021.121263.

Chen, M., Pang, D., Chen, X., Yan, H., and Yang, Y. (2022). Passive daytime radiative cooling: fundamentals, material designs, and applications. EcoMat *4*, 1–28. https://doi.org/10.1002/eom2.12153.

Chen, Y., Mandal, J., Li, W., Smith-Washington, A., Tsai, C.C., Huang, W., Shrestha, S., Yu, N., Han, R.P.S., Cao, A., and Yang, Y. (2020). Colored and paintable bilayer coatings with high solar-infrared reflectance for efficient cooling. Sci. Adv. *6*, eaaz5413. https://doi.org/10.1126/sciadv.aaz5413.

Chen, M., Pang, D., Mandal, J., Chen, X., Yan, H., He, Y., Yu, N., and Yang, Y. (2021b). Designing mesoporous photonic structures for high-performance passive daytime radiative cooling. Nano Lett. *21*, 1412–1418. https://doi.org/10.1021/acs.nanolett.0c04241.

Chen, Z., Zhu, L., Raman, A., and Fan, S. (2016). Radiative cooling to deep sub-freezing temperatures through a 24-h day-night cycle. Nat. Commun. *7*, 13729. https://doi.org/10.1038/ncomms13729.

Cheng, Z., Han, H., Wang, F., Yan, Y., Shi, X., Liang, H., Zhang, X., and Shuai, Y. (2021). Efficient radiative cooling coating with biomimetic human skin wrinkle structure. Nano Energy *89*, 106377. https://doi.org/10.1016/j.nanoen.2021.106377.

Fuqiang, W. (2020). Optical properties and cooling performance analyses of single-layer radiative cooling coating with mixture of TiO2 particles and SiO2 particles. Sci. China Technol. Sci. *64*, 1017–1029.

Hsu, P.C., Song, A.Y., Catrysse, P.B., Liu, C., Peng, Y., Xie, J., Fan, S., and Cui, Y. (2016). Radiative human body cooling by nanoporous polyethylene textile. Science *353*, 1019–1023. https://doi.org/10.1126/science.aaf5471.

Huang, Z., and Ruan, X. (2017). Nanoparticle embedded double-layer coating for daytime radiative cooling. Int. J. Heat Mass Transf. *104*, 890–896. https://doi.org/10.1016/j.ijheatmasstransfer.2016.08.009.

Incropera, F.P., and Dewitt, D.P. (2002). Fundamentals of Heat and Mass Transfer (York: Wiley).

Kim, H., and Lenert, A. (2018). Optical and thermal filtering nanoporous materials for sub-ambient radiative cooling. J. Opt. *20*. https://doi.org/10.1088/2040-8986/aacaa1.

Kou, J., Jurado, Z., Chen, Z., Fan, S., and Minnich, A.J. (2017). Daytime radiative cooling using near-black infrared emitters. ACS Photonics *4*, 626–630. https://doi.org/10.1021/acsphotonics.6b00991.

Leroy, A., Bhatia, B., Kelsall, C.C., Castillejo-Cuberos, A., Capua, M.D.H., Zhao, L., Zhang, L., Guzman, A.M., and Wang, E.N. (2019). High-performance subambient radiative cooling enabled by optically selective and thermally insulating polyethylene aerogel. Sci. Adv. *5*, 1–9. https://doi.org/10.1126/sciadv.aat9480.

Leroy, A., Bhatia, B., Sircar, J., and Wang, E.N. (2022). Thermal transport in solar-reflecting and infrared-transparent polyethylene aerogels. Int. J. Heat Mass Transf. *184*, 122307. https://doi.org/10.1016/j.ijheatmasstransfer.2021.122307.

Li, W., Buddhiraju, S., and Fan, S. (2020a). Thermodynamic limits for simultaneous energy harvesting from the hot sun and cold outer space. Light Sci. Appl. *9*, 68. https://doi.org/10.1038/s41377-020-0296-x.

Li, X., Peoples, J., Huang, Z., Zhao, Z., Jun, Q., and Ruan, X. (2020b). Full daytime sub-ambient radiative cooling with high figure of merit in commercial-like paints. Cell Rep. Phys. Sci. *1*, 100221.

Liu, J., Zhang, J., Tang, H., Zhou, Z., Zhang, D., Ye, L., and Zhao, D. (2021). Recent advances in the development of radiative sky cooling inspired from solar thermal harvesting. Nano Energy *81*, 105611. https://doi.org/10.1016/j.nanoen.2020.105611.

Liu, J., Zhou, Z., Zhang, J., Feng, W., and Zuo, J. (2019). Advances and challenges in commercializing radiative cooling. Mater. Today Phys. *11*, 100161. https://doi.org/10.1016/j.mtphys.2019.100161.

Ma, H., Wang, L., Dou, S., Zhao, H., Huang, M., Xu, Z., Zhang, X., Xu, X., Zhang, A., Yue, H., et al. (2021). Flexible daytime radiative cooling enhanced by enabling three-phase composites with scattering interfaces between silica microspheres and hierarchical porous coatings. ACS Appl. Mater. Interfaces. https://doi.org/10.1021/acsami.1c02145.

Mahian, O., Bellos, E., Markides, C.N., Taylor, R.A., Alagumalai, A., Yang, L., Qin, C., Lee, B.J., Ahmadi, G., Safaei, M.R., and Wongwises, S. (2021). Recent advances in using nanofluids in renewable energy systems and the environmental implications of their uptake. Nano Energy *86*, 106069. https://doi.org/10.1016/j.nanoen.2021.106069.

Mandal, J., Fu, Y., Overvig, A.C., Jia, M., Sun, K., Shi, N.N., Zhou, H., Xiao, X., Yu, N., and Yang, Y. (2018). Hierarchically porous polymer coatings for highly efficient passive daytime radiative cooling. Science *362*, 315–319. https://doi.org/10.1126/science.aat9513.

Mandal, J., Mandal, S., Brewer, J., Ramachandran, A., and Raman, A.P. (2020). Radiative cooling and thermoregulation in the earth's glow. Preprint at arXiv. https://doi.org/10.48550/arXiv.2006.11931.

Peng, Y., Chen, J., Song, A.Y., Catrysse, P.B., Hsu, P.C., Cai, L., Liu, B., Zhu, Y., Zhou, G., Wu, D.S., et al. (2018). Nanoporous polyethylene microfibres for large-scale radiative cooling fabric. Nat. Sustain. *1*, 105–112. https://doi.org/10.1038/s41893-018-0023-2.

Raman, A.P., Anoma, M.A., Zhu, L., Rephaeli, E., and Fan, S. (2014). Passive radiative cooling below ambient air temperature under direct sunlight. Nature *515*, 540–544. https://doi.org/10.1038/nature13883.

Smith, D.R., and Loewenstein, E.V. (1975). Optical constants of far infrared materials 3: plastics. Appl. Opt. *14*, 1335–1341. https://doi.org/10.1364/ao.14.001335.

Tian, Y., Liu, X., Chen, F., and Zheng, Y. (2021). A facile approach to achieve subambient radiative cooling through aluminum foils and polyethylene bubble wrap. Sol. Energy Mater. Sol. Cells *230*, 111286. https://doi.org/10.1016/j.solmat.2021.111286.

Wang, T., Wu, Y., Shi, L., Hu, X., Chen, M., and Wu, L. (2021). A structural polymer for highly efficient all-day passive radiative cooling. Nat. Nat. Commun. *12*, 365. https://doi.org/10.1038/s41467-020-20646-7.

Weng, Y., Zhang, W., Jiang, Y., Zhao, W., and Deng, Y. (2021). Effective daytime radiative cooling via a template method based PDMS sponge emitter with synergistic thermo-optical activity. Sol. Energy Mater. Sol. Cells *230*, 111205. https://doi.org/10.1016/j.solmat.2021.111205.

Xiang, B., Zhang, R., Luo, Y., Zhang, S., Xu, L., Min, H., Tang, S., and Meng, X. (2021). 3D porous polymer film with designed pore architecture and auto-deposited SiO2 for highly efficient passive radiative cooling. Nano Energy *81*, 105600. https://doi.org/10.1016/j.nanoen.2020.105600.

Yang, Y., and Zhang, Y. (2020). Passive daytime radiative cooling: Principle, application, and economic analysis. MRS Energy Sustain *7*, 5–8. https://doi.org/10.1557/mre.2020.18.

Yu, Z., Nie, X., Yuksel, A., and Lee, J. (2020). Reflectivity of solid and hollow microsphere composites and the effects of uniform and varying diameters. J. Appl. Phys. *128*. https://doi.org/10.1063/5.0015650.

Zhai, Y., Ma, Y., David, S.N., Zhao, D., Lou, R., Tan, G., Yang, R., and Yin, X. (2017). Scalable-manufactured randomized glass-polymer hybrid metamaterial for daytime radiative cooling. Science *355*, 1062–1066. https://doi.org/10.1126/science.aai7899.

Zhang, H., Ly, K.C.S., Liu, X., Chen, Z., Yan, M., Wu, Z., Wang, X., Zheng, Y., Zhou, H., and Fan, T. (2020). Biologically inspired flexible photonic films for efficient passive radiative cooling. Proc. Natl. Acad. Sci. USA *117*, 14657–14666. https://doi.org/10.1073/pnas.2001802117.

Zhang, J., Zhou, Z., Quan, J., Zhang, D., Sui, J., Yu, J., and Liu, J. (2021a). A flexible film to block solar radiation for daytime radiative cooling. Sol. Energy Mater. Sol. Cells *225*, 111029. https://doi.org/10.1016/j.solmat.2021.111029.

Zhang, J., Zhou, Z., Tang, H., Xing, J., Quan, J., Liu, J., Yu, J., and Hu, M. (2021b). Mechanically robust and spectrally selective convection shield for daytime subambient radiative cooling. ACS Appl. Mater. Interfaces. https://doi.org/10.1021/acsami.0c21204.

Zhang, S., Jing, W., Chen, Z., Zhang, C., Wu, D., Gao, Y., and Zhu, H. (2022). Full daytime sub-ambient radiative cooling film with high efficiency and low cost. Renew. Energy *194*, 850–857. https://doi.org/10.1016/j.renene.2022.05.151.

Zhao, D., Aili, A., Zhai, Y., Xu, S., Tan, G., Yin, X., and Yang, R. (2019). Radiative sky cooling:

fundamental principles, materials, and applications. Appl. Phys. Rev. *6*, 021306. https://doi.org/10.1063/1.5087281.

Zhao, Y., Pang, D., Chen, M., Chen, Z., and Yan, H. (2022). Scalable aqueous processing-based radiative cooling coatings for heat dissipation applications. Appl. Mater. Today *26*, 101298. https://doi.org/10.1016/j.apmt.2021.101298.

Zhong, S., Yi, L., Zhang, J., Xu, T., Xu, L., Zhang, X., Zuo, T., and Cai, Y. (2021). Self-cleaning and spectrally selective coating on cotton fabric for passive daytime radiative cooling. Chem. Eng. J. *407*, 127104. https://doi.org/10.1016/j.cej.2020.127104.

Zhou, L., Song, H., Liang, J., Singer, M., Zhou, M., Stegenburgs, E., Zhang, N., Xu, C., Ng, T., Yu, Z., et al. (2019). A polydimethylsiloxane-coated metal structure for all-day radiative cooling. Nat. Sustain. *2*, 718–724. https://doi.org/10.1038/s41893-019-0348-5.

Zhu, L., Raman, A., and Fan, S. (2013). Color-preserving daytime radiative cooling. Appl. Phys. Lett. *103*, 223902. https://doi.org/10.1063/1.4835995.

STAR★METHODS

KEY RESOURCES TABLE

REAGENT or RESOURCE	SOURCE	IDENTIFIER
Chemicals, peptides, and recombinant proteins		
HDPE	Taotao plastic materials Co.,Ltd	N/A
UHMWPE	Taotao plastic materials Co.,Ltd	N/A
Paraffin oil	Aladdin	P104801
Anhydrous ethanol	Aladdin	E111989
Other		
Spectrometer	Ideaoptics	PG2000 and NIR1700
Fourier infrared spectroscope	Thermo Scientific	Nicolet iS50
Scanning Electron Microscope	TESCAN	Clara eds: Xplore 30
Thermocouples	Kaipusen	TTK36
Solar power meter	TES	TES-1333R
Acquisition instrument	Keysight	34970A

RESOURCE AVAILABILITY

Lead contact

Further information and requests for resources and reagents should be directed to and will be fulfilled by the lead contact, Meijie Chen.

Materials availability

This study did not generate new unique reagents.

Data availability

- Data will be made available on request.
- This paper does not report the original code.
- Any additional information required to reanalyze the data reported in this paper is available from the lead contact upon request.

METHOD DETAILS

Preparation of P-PE coatings

The P-PE coating was fabricated by mixing high-density PE (HDPE) and ultrahigh molecular weight PE (UHMWPE) at a certain weight ratio in paraffin oil at 160°C for 30 min using an overhead stirrer and then vacuum heated at 180°C for 6 h to obtain a homogeneous polymer mixture. The mixture was then melt-pressed into a thin film. Finally, using the anhydrous ethanol (99%) to extract the paraffin oil and an interconnected porous polymer network is created.

Sample characterizations

The image of P-PE was taken with a camera. The SEM image was taken by a MIRA4 LMH TESCAN SEM (5kV). The thickness of coatings was measured by an electronic micrometer. The spectral reflectance and transmittance of coatings were determined separately in the near-infrared (0.37–1.7 μm) and near-infrared to mid-infrared (1.7–17 μm). The first range was measured using a fiber optic spectrometer from ideaoptics (PG2000 for 0.37–1.0 μm and NIR1700 for 1.0–1.7 μm) equipped with an integrating sphere (IS-50-10-R) using a diffuse standard whiteboard (JY-WS1) as the reference. And the second range is measured by a Fourier transform infrared spectroscope (Nicolet iS50) with a gold integrating sphere and Mercury-Cadmium-Telluride detector (Pike Technologies) and a gold sample was used for reference. The tensile strength test

was measured by an MTS 249. The width and thickness of the sample size are 1 cm and 100 μm. The displacement rate was 10 mm min^{-1}.

Water vapor transmission property tests

The test was based on ASTME96-2014 with modification. Plastic bottles (50mL) were filled with 30 mL of distilled water and sealed with the P-PE coating using PE tape. The exposed area of PE coating was 4.9 cm^2. The sealed bottles were heated at 35°C and the relative humidity was 74%. The mass of sealed bottles was measured every hour. By dividing the reduced mass of water by the exposed area of the bottle (4.9 cm^2) and time (one hour), the water vapor transmission was calculated. Water vapor transmission rate (WVTR) represents the weight of water vapor transmission from the material under a certain time, temperature, and humidity, which can be defined as $WVTR = G/tA$, and G is the weight change of water, t is time for weight change, A is the area of coatings.

Field tests

The outdoor experiment was conducted on the rooftop of a building at Central South University (Changsha, China), on May 2, 2022. Human skin was simulated by a silicone rubber that has IR emissivity similar to human skin (Figure S4) which was placed in the foam groove (4 cm × 4 cm × 4cm) where the foam is covered with Al foil to minimize the influence of convective and conductive heat transfer from the surroundings and the aluminum foil can minimize the influence of solar irradiation. The coating was placed 2 cm above the silicone rubber to reflect sunlight. Thermocouples (T-type) connected to the acquisition instrument were in contact with the top surface of the rubber to measure the simulated skin temperature. In addition, a thermocouple under shade recorded the ambient temperature to avoid the influence of direct sunlight. A data-logging solar power meter was used to record the direct and diffuse solar irradiance. All measurement data was transferred to a laptop through an acquisition instrument.

Heat dissipation calculation

The solar reflectance $\overline{R}_{solar}$ was calculated as the ratio of the reflected solar intensity across the solar spectrum (λ = 0.3–2.5 μm) to the integral solar intensity in the same range, as shown below:

$$\overline{R}_{solar} = \frac{\int_{\lambda_1}^{\lambda_2} I_{solar}(\lambda) R(\lambda) d\lambda}{\int_{\lambda_1}^{\lambda_2} I_{solar}(\lambda) d\lambda}, \quad \text{(Equation 1)}$$

where $I_{solar}(\lambda)$ represented the ASTM G173-03 Global solar intensity spectrum at AM 1.5, $R(\lambda)$ was the spectral reflectance.

The averaged thermal emittance $\overline{\varepsilon}_{LWIR}$ and transmittance $\overline{\tau}_{LWIR}$ in the atmospheric transmission window were calculated as:

$$\overline{\varepsilon}_{LWIR} = \frac{\int_{8\mu m}^{13\mu m} I_{bb}(T,\lambda)\varepsilon(\lambda) d\lambda}{\int_{8\mu m}^{13\mu m} I_{bb}(T,\lambda) d\lambda}, \quad \text{(Equation 2)}$$

$$\overline{\tau}_{LWIR} = \frac{\int_{8\mu m}^{13\mu m} I_{bb}(T,\lambda)\tau(\lambda) d\lambda}{\int_{8\mu m}^{13\mu m} I_{bb}(T,\lambda) d\lambda}, \quad \text{(Equation 3)}$$

where $I_{bb}(T, \lambda)$ was the spectral intensity emitted by a standard blackbody with a temperature of T (25°C), $\varepsilon(\lambda)$ and $\tau(\lambda)$ represented the sample's spectral emittance and transmittance.

The temperature based on the IR transparent and normal PDRC coatings was simulated using the commercial software package COMSOL Multiphysics. The size is 20 cm × 10 cm and the coating has the same size as the heater. The natural convection inside is not considered, and the convection heat transfer coefficient outside is 5 W m^{-2} K^{-1}. $\overline{\varepsilon}_{LWIR}$ of the normal PDRC coating is 1. $\overline{\tau}_{LWIR}$ of the IR-transparent coating is 1. And the other boundaries have a reflectance of 1 to reflect the thermal radiation from the heater and normal PDRC coating. The governing equations are shown below:

$$\rho c_p \mathbf{u} \cdot \nabla T + \nabla \mathbf{q} = -Q + q_0, \quad \text{(Equation 4)}$$

$$\mathbf{q} = -k \nabla T, \quad \text{(Equation 5)}$$

$$Q = P_{rad}(T) - P_{atm}(T_{atm}), \quad \text{(Equation 6)}$$

$$P_{\mathrm{rad}}(T) = 2\pi \int \mathrm{d}\Omega \cos\theta \int_0^{\infty} \mathrm{d}\lambda \varepsilon(\theta,\lambda) I_{\mathrm{bb}}(T,\lambda), \quad \text{(Equation 7)}$$

$$P_{\mathrm{atm}}(T_{\mathrm{atm}}) = \int \cos\theta \mathrm{d}\Omega \int_0^{\infty} \mathrm{d}\lambda \varepsilon(\theta,\lambda) \varepsilon_{\mathrm{atm}}(\theta,\lambda) I_{\mathrm{bb}}(T_{\mathrm{atm}},\lambda), \quad \text{(Equation 8)}$$

where ρ, c_p, and $\mathbf{u}$ are the density, specific heat capacity, and velocity. ∇T is the temperature gradient. $\mathbf{q}$ is heat flux by thermal conduction. Q is heat flux by thermal radiation. q_0 is the heating power of the heater. $P_{rad}(T)$ is the total radiative power from the heater. $P_{atm}(T_{atm})$ is the atmospheric radiation absorbed by the heater and the ambient temperature T_{atm} is 25°C.